https://doi.org/10.1016/j.solener.2021.10.057 This is the Pre-Published Version.

The following publication Shen, B., Ding, S., Wang, Y., Lu, L., & Yang, H. (2021). Novel one-pot solvothermal synthesis and phase-transition mechanism of hexagonal CsxWO3 nanocrystals with superior near-infrared shielding property for energy-efficient windows. Solar Energy, 230, 401-408 is available at https://doi.org/10.1016/j.solener.2021.10.057.

Novel one-pot synthesis and growth mechanism of hexagonal Cs_xWO_3 nanocrystals with superior near-infrared shielding property for energy-efficient windows

Boxu Shen[1]*, Yuanhao Wang[2,]*, Lin Lu[1], Hongxing Yang[1]

1. Renewable Energy Research Group (RERG), Department of Building Services Engineering, The Hong Kong Polytechnic University, Kowloon, Hong Kong

2. SUSTech Engineering Innovation Center, School of Environmental Science and Engineering, Southern University of Science and Technology, Shenzhen, Guangdong 518055, China

*Corresponding author: Boxu Shen; Yuanhao Wang

E-mail addresses: boxushen.shen@connect.polyu.hk (B. Shen);

yuanhaowang@yahoo.com, wangyh2020@mail.sustech.edu.cn (Y. Wang)

Abstract

The controllable one-pot synthesis of hexagonal Cs_xWO_3 nanocrystals without post heat-treatment remains a great challenge in the field of nanocrystal materials. In this study, a facile one-pot method for controllable synthesis of Cs_xWO_3 nanocrystals using stable and relatively cheap ammonium metatungstate and cesium carbonate as starting materials was proposed. The reducibility of tartaric acid, tartaric acid with chloroplatinic acid were studied, and the possible synthetic mechanisms of Cs_xWO_3 nanocrystals with different crystalline phase were discussed in detail. The results indicate that tartaric acid with the presence of chloroplatinic acid could promote the formation of most W^{5+} ions in the hexagonal Cs_xWO_3 nanocrystals. Especially, when the solid content of the dispersion reached 6 wt%, the ordinary glass with the coating demonstrated the average visible light transmittance of 71.76% and the average near-infrared shielding ratio of 85.64%. This work is of great significance for synthesizing low-cost hexagonal Cs_xWO_3 nanocrystals without post heat-treatment and promoting the development of energy-efficient

windows.

Keywords: novel one-pot synthesis, growth mechanism, hexagonal Cs_xWO_3 nanocrystals, near-infrared shielding property, energy-efficient windows, ammonium metatungstate hydrate

1. Introduction

The building sector makes up 36 % of the global final energy use and 28 % of energy-related carbon emission in 2019 as the largest contributor in the world [1, 2]. Heating, ventilation, and air conditioning (HVAC) systems, actually account for half of the building energy consumption [3]. The largest contributor of the heat gain in buildings for cooling load in summer is solar radiation passing through windows [4-6]. A window can be divided into two parts: the glazing materials, which accounts for 80-90% of its area, and the framework, which is applied to sustain the glass pane on the building walls and to act as a peripheral seal [7, 8]. Sunlight is composed of ultraviolet, visible light and near-infrared light in the range of 300-2500 nm. Among them, near-infrared light is invisible radiation, accounting for about 50% of the total solar energy [9, 10]. Ordinary glasses lack the spectral selectivity with solar transmittance of 75 % to 90 % [11]. Thus, the development of spectrally selective material for energy-efficient glazing has been one of the effective means to reduce electricity consumption of air-conditioning and corresponding CO_2 emission [8].

Energy-efficient glazing is usually fabricated by functional layers composed of spectrally selective materials, which can change the way the glass interacting with solar radiation [12]. Until now, most commonly used materials for energy-efficient glazing comprise silver (Ag) and transparent conductive oxides (TCOs). Generally, the silver-based Low-E coating is fabricated by the vacuum sputter method [9, 13]. Although it exhibits quite good spectrally selective performance, the extra cost of one more glass pane and encapsulating configuration, the complex fabrication

procedure with slow sputter rate and the use of noble metals make it hard to conduct window retrofit for existing buildings [14]. As for TCOs, tin-doped indium oxide (ITO) and antimony-doped tin oxide (ATO) are the most frequently reported spectrally selective materials for energy-efficient glazing [15-19]. However, ITO and ATO still exhibited high transmittance below the near-infrared wavelength of 1500 nm [20, 21]. Besides, indium used in ITO is a kind of rare metal resource, which is not conducive to industrial production [22]. Recently, hexagonal tungsten bronze nanocrystals (M_xWO_3, M = Na, K, Rb, Cs, NH_4) have been reported as a novel type of spectrally selective material with strong localized surface plasmon resonance (LSPR) [23-25]. Especially for cesium doped hexagonal tungsten nanocrystals (Cs-HTBs), it has been proved that the Cs-HTBs-based film exhibited excellent shielding performance below the wavelength of 1500 nm [26]. However, cesium doped tungsten bronze nanocrystals (Cs_xWO_3) have different phase types, which significantly affects its spectral selectivity [27]. Therefore, the controllable synthesis of cesium doped tungsten bronze with the desired crystalline phase is of great significance for its practical application.

At present, the synthesis of Cs-HTBs mainly includes solid-state reaction and liquid-phase method. Generally, Cs-HTBs prepared by conventional solid-state reaction requires a heat-treatment in H_2/N_2 mixed atmosphere for improving the crystallinity of the products, but the high reaction temperature tends to cause a larger and uneven particle size, which is adverse to the dispersion of Cs-HTBs and the optical property of their films [28-30]. The conventional solid-state reaction is also considered dangerous due to the use of H_2 which is flammable and explosive. Moreover, Cs-HTBs can be prepared through solvothermal method using WCl_6 and $CsOH{\bullet}H_2O$ as starting materials [21, 23, 31]. Although this method avoids the heat-treatment in the dangerous H_2/N_2 atmosphere, the starting materials are not favorable for scalable work because of high cost,

inconvenient storage and insufficient environment-friendly. In addition, the synthesis of Cs-HTBs was investigated by liquid-phase method using sodium tungstate (Na_2WO_4•H_2O) and cesium sulfate (Cs_2SO_4) as starting materials [25, 32-35]. Although the inexpensive and stable raw materials are suitable for industrial application, Na_2WO_4•H_2O still needs to be pretreated to obtain the gel-like tungstate acid suspension and post heat-treatment is still required. The pretreatment in this method will increase cost, and the post heat-treatment will cause the secondary growth of Cs-HTBs which is not favorable for its optical performance. Therefore, it is necessary to prepare Cs-HTBs with excellent optical property by one-pot process without needing any post heat-treatment using cheap and stable raw materials.

In this study, controllable one-pot synthesis of Cs-HTBs without post heat-treatment was proposed using ammonium metatungstate hydrate (AMT) as the W source and cesium carbonate (Cs_2CO_3) as Cs source. The reducing mechanism of the tartaric acid and the tartaric acid with the assistance of the chloroplatinic acid for the synthesis of Cs-HTBs was studied. The relationships between the different reducing agents used in the synthetic process and the crystalline composition of the as-prepared nanocrystals were discussed and the possible synthesis mechanism was subsequently proposed. This synthetic strategy is of great implication for reducing costs of production and pushing the application of Cs-HTBs in the field of energy-efficient glazing.

2. Experimental study

2.1 Materials

Ammonium metatungstate hydrate (AMT, $(NH_4)_6H_2W_{12}O_{40}\cdot aH_2O$), cesium carbonate ($Cs_2CO_3$), tartaric acid ($C_4H_6O_6$), chloroplatinic acid ($H_2PtCl_6$), deionized water ($H_2O$), anhydrous ethanol ($C_2H_5OH$), polyethylene glycol 200 (PEG 200) and polyvinyl alcohol (PVA) were purchased from

Macklin.

2.2 Synthesis of Cs_xWO_3 nanocrystals

Cs_xWO_3 were composed via the solvothermal method using AMT as W source and Cs_2CO_3 as Cs source respectively. Typical procedures were as follows. A certain amount of AMT was put into the solvent, then Cs_2CO_3 was added into the solution of AMT with a Cs/W molar ratio of 0.33. The total volume of the mixed solution was 30 ml. After that the as-prepared solution was transferred into the Teflon-lined autoclave of 50 ml interval volume, followed by solvothermal reaction in a drying oven at 240 ℃ for 24 hours. The obtained blue products were collected by centrifugation and washed three times with ethanol and finally dried at 60 ℃ in vacuum. The Cs_xWO_3 nanocrystals synthesized by absolute ethanol were named as CWO-1. The Cs_xWO_3 nanocrystals synthesized by anhydrous ethanol with tartaric acid of 1 mol/L in the precursor solution were named as CWO-2. The Cs_xWO_3 nanocrystals prepared by ethanol with 1 mol/L tartaric acid and a certain amount of chloroplatinic acid were labelled as CWO-3. The corresponding products doped without Cs_2CO_3 in the precursors were obtained and labelled as WO-1, WO-2 and WO-3.

2.3 Fabrication of Cs_xWO_3/PVA coatings

Cs_xWO_3/PVA coatings were fabricated by a simple blending process. PVA powders were selected as film former. Detailed preparation steps of Cs_xWO_3/PVA coatings were as follows. First, PVA powders were dissolved in deionized water to form a homogeneous dispersion with 4wt%. After that, Cs_xWO_3 were added in the above dispersion with continuous mixing for 2 h. The as-prepared dispersion was then sprayed on the ordinary glazing surface to fabricate the Cs_xWO_3/PVA coatings.

2.4 Characterization

The phase compositions of Cs_xWO_3 were investigated by means of X-ray diffraction (XRD) with

Cu Kα radiation. The morphologies of the nanocrystals were observed by transmission electron microscopy (TEM) with an energy dispersive spectrum (EDS) attachment. The chemical composition and binding energies of W 4f were examined by X-ray photoelectron spectroscopy (XPS). UV-vis-NIR spectrophotometer was used to measure the optical parameters of the composite coatings.

3. Results and discussion

Fig. 1 presents the XRD patterns of the as-prepared Cs_xWO_3 (CWO-1, CWO-2 and CWO-3) nanocrystals with different reducing agents and a mixed (hexagonal and cubic) phase appears in CWO-1 and CWO-2. Fig. 2 shows the structural frameworks of cesium doped hexagonal tungsten bronze nanocrystals (Cs-HTBs) and cesium doped cubic tungsten bronze nanocrystals (Cs-CTBs). Cs-HTBs shown in Fig. 2a consist of corner-sharing WO_6 octahedral arrays with Cs^+ ions located in the hexagonal channels of the crystal framework. The upper limit of Cs/W is 0.33 in hexagonal system when Cs^+ ions are fully doped. It has been proved that Cs-HTBs illustrate strong localized surface plasmon resonance (LSPR) phenomenon which is the crucial property of Cs-HTBs to shield the near-infrared radiation from the sunlight. As for Cs-CTBs shown in Fig. 2b, it can be seen that the Cs^+ ions are located in the cubic channels and the strong LSPR of Cs-HTB is different from that of Cs-CTB.

The XRD pattern of CWO-1 can be well indexed to the mixed crystal phase of cubic $(Cs_2O)_{0.44}W_2O_6$ (JCPDS 47-0566) and hexagonal $Cs_{0.2}WO_3$ (JCPDS 83-1333). CWO-1 were prepared in absolute ethanol without any other reducing additives. The results reveal that absolute ethanol cannot fully promote the synthesis of hexagonal phase nanocrystals and thus the doping of Cs^+ ions is restricted. As for CWO-2, a small diffraction peak belonging to cubic $(Cs_2O)_{0.44}W_2O_6$

(JCPDS 47-0566) was observed and other diffraction peaks of CWO-2 agreed well with the hexagonal diffraction peaks of $Cs_{0.3}WO_3$ (JCPDS 81-1244). CWO-2 were synthesized by tartaric acid in absolute ethanol. The results indicate that more Cs^+ ions entered into the hexagonal tunnels of the crystal structure due to the stronger reducibility of tartaric acid, but cubic phase still existed in the as-synthesized nanocrystals. Fig. 3a shows the synthetic process of Cs-HTBs reduced by tartaric acid. The two carboxyl groups of tartaric acid tended to conduct decarboxylation under the stimulation of α-hydroxyl group and β-hydroxyl group. The generated free hydrogen atoms ([H]) with strong reducibility took the oxygen atoms of $[WO_6]$ octahedrons to change W^{6+} ions into W^{5+} ions, which promoted Cs^+ ions entering into the crystal structure. It can be seen that the XRD pattern of CWO-3 was well indexed to the pure hexagonal $Cs_{0.33}WO_3$ (JCPDS 83-1334), suggesting that the most Cs^+ ions are doped into the lattice structure. CWO-3 were obtained in absolute ethanol with the presence of tartaric acid and chloroplatinic acid. Fig. 3b presents the process of chloroplatinic acid enhancing the reducibility of tartaric acid in the controllable one-pot synthesis, and the role of the chloroplatinic acid here was regarded as Pt-catalysis. The mechanism of Pt-catalysis can be described as follows. Firstly, Pt^{4+} ions derived from chloroplatinic acid obtained free electrons and was reduced to metallic platinum by tartaric acid. Subsequently, H^+ ions decomposed from tartaric acid got electrons from metallic platinum and turned into [H] with higher reducibility, while metallic platinum lost electrons and transformed Pt^{4+} ions again. Finally, the produced [H] with higher reducibility took the oxygen atoms of $[WO_6]$ octahedrons to generate H_2O and oxygen vacancies, while W^{6+} ions turned into W^{5+} ions by getting electrons originated from oxygen vacancies. Thus, the charge imbalance caused by W^{5+} ions promoted Cs^+ ions entering into the lattice structure to form hexagonal phase. It is suggested that the reducibility of the reducdtant plays a crucial role to

the formation of hexagonal phase, which indicates that Pt-catalysis facilitates the reduction reaction and causes the doping level of Cs^+ ions to a higher degree. In addition, it is found that the diffraction peak intensity increased in the order of CWO-1, CWO-2 and CWO-3, indicating that the reductant with higher reducibility stimulate the growth of nanocrystals and cause a higher crystallinity.

As inspired by the reduction mechanism shown in Fig. 3b, the chemical reaction was described by the following equations. Firstly, AMT (Ammonium metatungstate hydrate) resolved into WO_3, NH_3 and H_2O with the increase of reaction temperature. The Oxalaldehyde ($C_2H_2O_2$), carbon dioxide (CO_2) and hydrogen ions (H^+) were the by-products of tartaric acid after the reaction. H_2O was obtained by the combination of the [H] and oxygen atoms of [WO_6]. The product presented by $Cs_{0.33}WO_{2.835}$ was used to balance the reaction equation, and it is generally believed that Cs-HTBs were defined as $Cs_{0.33}WO_3$.

$$(NH_4)_6H_2W_{12}O_{40}\cdot aH_2O \rightarrow 6NH_3 + 12WO_3 + (a+4)H_2O$$

$$WO_3 + 0.33Cs^+ + 0.165C_4H_6O_6 \rightarrow Cs_{0.33}WO_{2.835} + 0.165C_2H_2O_2 + 0.33H^+ + 0.33CO_2 + 0.165H_2O$$

The chemical composition and W valence state were determined by XPS. Fig. 4a shows the survey spectra of CWO-1, CWO-2 and CWO-3. All the spectra confirm the presence of Cs, W and O elements. As shown in Fig. 4b, the difference of Cs 3d characteristic peak position suggests that the Cs^+ ions chemical environment in CWO-1, CWO-2 and CWO-3 changes with the different reductant. Cs^+ ions were surrounded by O atoms with a certain degree of electronegativity in the hexagonal structure. The results suggest that more Cs^+ ions enter into the hexagonal tunnel then Cs 3d characteristic peak position moves to the higher binding energy direction. Thus, more Cs^+ ions existed in the hexagonal tunnels of CWO-3.

Fig. 5a-c display the W 4f core-level spectra of CWO-1, CWO-2 and CWO-3 synthesized using

different reductants. The spin-orbital peaks located at 34.2 eV/ 36.7 eV and 35.8 eV/37.9 eV can be attributed to W^{5+} and W^{6+} respectively. As shown in Fig. 5d, the content of W^{5+} in CWO-3 is the largest, accounting for 32% of total W atoms. This indicates that the increase of W^{5+} generation is caused by more Cs^+ ions insertion, which plays a positive influence on the NIR shielding performance based on localized surface plasmon resonance (LSPR) [20].

Fig. 6 shows the XRD patterns of WO-1, WO-2 and WO-3, which correspond to CWO-1, CWO-2 and CWO-3 without Cs doping. It can be seen that the XRD pattern of WO-1 agreed well with the hexagonal $(NH_4)_{0.25}WO_3$ (JCPDS 73-1084), indicating that NH_4^+ ions can be effectively doped into the crystal structure without Cs sources. As for WO-2 and WO-3, the two XRD patterns presented a mixed phase composition. The appearance of $WO_3 \cdot 0.33H_2O$ (JCPDS 35-1001) indicates that the addition of tartaric acid is not conducive for NH_4^+ ions entering into the crystal structure. In other words, tartaric acid can promote Cs^+ ions into the crystal structure even in the presence of NH_4^+ ions. In addition, it is found that the characteristic peak intensity of WO-3 slightly increased compared with that of WO-2, suggesting that Pt-catalysis can facilitate the growth of nanocrystals.

According to the discussion above, a brief diagram of synthetic routes is shown in Fig. 7. It is found that the presence of Cs and W source was the prerequisite to prepare desired phase samples. Moreover, the phase composition was determined by the reducibility of reducing agents. It can be seen that a mixed composition of hexagonal and cubic phase was obtained in ethanol or ethanol with tartaric acid, indicating that the reducibility of the two conditions is not enough to prepare nanocrystals with a pure hexagonal phase. When chloroplatinic acid was added, the Cs-HTBs were successfully synthesized due to the improved reducibility assisted by Pt-catalysis.

As shown in Fig. 8a, the nanocrystals show rectangle-like shape with a certain extent of

agglomeration. Fig. 8b presents the lattice spacing of 0.391 nm and 0.338 nm, which corresponds to the plane of (002) and (111) respectively. The hexagonal structure of CWO-3 was further verified by the SAED pattern in Fig. 8c. Fig. 8d presents element composition and indicates the existence of Cs, W and O element. Besides, the calculated Cs/W molar ratio is 0.3007, which is quite close to the upper limit of 0.33 for Cs-HTBs.

To fabricate the CWO-3/PVA composite films, the as-synthesized CWO-3 nanoparticles were mixed with PVA solution. Fig. 9 shows the samples fabricated by the dispersion with 2 wt%, 4 wt%, 6 wt% and 8 wt% respectively. To evaluate the spectral selectivity of the samples, we proposed three parameters, involving T_{Vis}, T_{NIR} and K (spectrally selective index defined as $K = T_{Vis} / T_{NIR}$) [36, 37]. Above calculated values are presented in Table 1. It is found that the solid content played a significant effect on improving optical property. Specifically, higher K means better optical properties. As displayed in Table 1, T_{NIR} declined as the solid content increased, suggesting better spectral selectivity. When the solid content reach 8 wt%, T_{Vis} was below 70%, which is adverse to daylight for windows. Thus, we concluded that the composite coating with the solid content of 6 wt% exhibited better comprehensive spectral selectivity than the films with other solid content.

4. Conclusions

Hexagonal Cs_xWO_3 nanocrystals were successfully prepared by controllable solvothermal method using stable and relatively cheap ammonium metatungstate and cesium carbonate as raw materials. Tartaric acid with the presence of chloroplatinic acid as the reductant showed the strongest reducibility and could produce the most W^{5+} ions in the as-synthesized product. It has been proved that the chloroplatinic acid plays an important effect on improving the reducibility of tartaric acid. Moreover, the CWO-3/PVA composite film fabricated by the dispersion with solid content of 6 wt%

displayed excellent near-infrared shielding performance with the average visible light transmittance of 71.76% and the average near-infrared shielding rate of 85.64% respectively. Furthermore, the novel one-pot synthesis without post heat-treatment for hexagonal Cs_xWO_3 nanocrystals is more suitable for industrial production, which is significant for the field of energy-efficient windows.

Declaration of competing interest

The authors declare that they have no known competing financial interests or personal relationships that could have appeared to influence the work reported in this paper.

Acknowledgements

This work was supported by the TCS project of the Hong Kong Innovation and Technology Fund (UIT/139) and Sola Green Technologies Limited. This work was also supported by the National Natural Science Foundation of China (Grant No. 61705258).

References

[1] Yue X, Zhang T, Yang D, Qiu F, Wei G, Zhou H. Multifunctional Janus fibrous hybrid membranes with sandwich structure for on-demand personal thermal management. Nano Energy. 2019;63.

[2] Yue X, Chen H, Zhang T, Qiu Z, Qiu F, Yang D. Controllable fabrication of tendril-inspired hierarchical hybrid membrane for efficient recovering tellurium from photovoltaic waste. Journal of Cleaner Production. 2019;230:966-73.

[3] Wei G, Yang D, Zhang T, Yue X, Qiu F. Fabrication of multifunctional coating with high luminous transmittance, self-cleaning and radiative cooling performances for energy-efficient windows. Solar Energy Materials and Solar Cells. 2019;202.

[4] Zhou Y, Li N, Xin Y, Cao X, Ji S, Jin P. CsxWO3 nanoparticle-based organic polymer transparent

foils: low haze, high near infrared-shielding ability and excellent photochromic stability. Journal of Materials Chemistry C. 2017;5:6251-8.

[5] Zeng X, Zhou Y, Ji S, Luo H, Yao H, Huang X, et al. The preparation of a high performance near-infrared shielding CsxWO3/SiO2composite resin coating and research on its optical stability under ultraviolet illumination. Journal of Materials Chemistry C. 2015;3:8050-60.

[6] Carboni M, Carravetta M, Zhang XL, Stulz E. Efficient NIR light blockage with matrix embedded silver nanoprism thin films for energy saving window coating. Journal of Materials Chemistry C. 2016;4:1584-8.

[7] Rezaei SD, Shannigrahi S, Ramakrishna S. A review of conventional, advanced, and smart glazing technologies and materials for improving indoor environment. Solar Energy Materials and Solar Cells. 2017;159:26-51.

[8] Gorgolis G, Karamanis D. Solar energy materials for glazing technologies. Solar Energy Materials and Solar Cells. 2016;144:559-78.

[9] Jelle BP, Kalnæs SE, Gao T. Low-emissivity materials for building applications: A state-of-the-art review and future research perspectives. Energy and Buildings. 2015;96:329-56.

[10] Hee WJ, Alghoul MA, Bakhtyar B, Elayeb O, Shameri MA, Alrubaih MS, et al. The role of window glazing on daylighting and energy saving in buildings. Renewable and Sustainable Energy Reviews. 2015;42:323-43.

[11] Garlisi C, Trepci E, Li X, Al Sakkaf R, Al-Ali K, Nogueira RP, et al. Multilayer thin film structures for multifunctional glass: Self-cleaning, antireflective and energy-saving properties. Applied Energy. 2020;264.

[12] Zheng L, Xiong T, Shah KW. Transparent nanomaterial-based solar cool coatings: Synthesis,

morphologies and applications. Solar Energy. 2019;193:837-58.

[13] Jelle BP, Hynd A, Gustavsen A, Arasteh D, Goudey H, Hart R. Fenestration of today and tomorrow: A state-of-the-art review and future research opportunities. Solar Energy Materials and Solar Cells. 2012;96:1-28.

[14] Fang Y, Hyde TJ, Arya F, Hewitt N, Wang R, Dai Y. Enhancing the thermal performance of triple vacuum glazing with low-emittance coatings. Energy and Buildings. 2015;97:186-95.

[15] Shen B, Wang Y, Lu L, Yang H. Synthesis and characterization of Sb-doped SnO2 with high near-infrared shielding property for energy-efficient windows by a facile dual-titration co-precipitation method. Ceramics International. 2020;46:18518-25.

[16] Wang M, Xu Y, Liu Y, Wu W, Xu S. Synthesis of Sb-doped SnO2 (ATO) hollow microspheres and its application in photo-thermal shielding coating. Progress in Organic Coatings. 2019;136.

[17] Maho A, Comeron Lamela L, Henrist C, Henrard L, Tizei LHG, Kociak M, et al. Solvothermally-synthesized tin-doped indium oxide plasmonic nanocrystals spray-deposited onto glass as near-infrared electrochromic films. Solar Energy Materials and Solar Cells. 2019;200.

[18] Shen B, Wang Y, Lu L, Yang H. Spraying fabrication of spectrally selective coating with improved near-infrared shielding performance for energy-efficient glazing. Ceramics International. 2021;47:18991-7.

[19] Shen B, Wang Y, Lu L, Yang H. pH-dependent doping level and optical performance of antimony-doped tin oxide nanocrystals as nanofillers of spectrally selective coating for energy-efficient windows. Ceramics International. 2021;47:20335-40.

[20] Song X, Liu J, Shi F, Fan C, Ran S, Zhang H, et al. Facile fabrication of KmCsnWO3 with greatly improved near-infrared shielding efficiency based on W5+-induced small polaron and local

surface plasmon resonance (LSPR) modulation. Solar Energy Materials and Solar Cells. 2020;218.

[21] Qi S, Xiao X, Lu Y, Huan C, Zhan Y, Liu H, et al. A facile method to synthesize small-sized and superior crystalline Cs0.32WO3 nanoparticles for transparent NIR shielding coatings. CrystEngComm. 2019;21:3264-72.

[22] Ran S, Liu J, Shi F, Fan C, Chen B, Zhang H, et al. Greatly improved heat-shielding performance of KxWO3 by trace Pt doping for energy-saving window glass applications. Solar Energy Materials and Solar Cells. 2018;174:342-50.

[23] Guo C, Yin S, Yan M, Sato T. Facile synthesis of homogeneous CsxWO3 nanorods with excellent low-emissivity and NIR shielding property by a water controlled-release process. Journal of Materials Chemistry. 2011;21.

[24] Xu X, Zhang W, Hu Y, Wang Y, Lu L, Wang S. Preparation and overall energy performance assessment of wide waveband two-component transparent NIR shielding coatings. Solar Energy Materials and Solar Cells. 2017;168:119-29.

[25] Liu J, Chen B, Fan C, Shi F, Ran S, Yang J, et al. Controllable synthesis of small size CsxWO3 nanorods as transparent heat insulation film additives. CrystEngComm. 2018;20:1509-19.

[26] Chao L, Bao L, Wei W, Tegus O. A review of recent advances in synthesis, characterization and NIR shielding property of nanocrystalline rare-earth hexaborides and tungsten bronzes. Solar Energy. 2019;190:10-27.

[27] Tahmasebi N, Madmoli S, Farahnak P. Synthesis of cesium tungsten bronze nanofibers with different crystalline phases. Materials Letters. 2018;211:161-4.

[28] Takeda H, Adachi K. Near Infrared Absorption of Tungsten Oxide Nanoparticle Dispersions. Journal of the American Ceramic Society. 2007;0:070922001254002-???

[29] Adachi K, Asahi T. Activation of plasmons and polarons in solar control cesium tungsten bronze and reduced tungsten oxide nanoparticles. Journal of Materials Research. 2012;27:965-70.

[30] Adachi K, Ota Y, Tanaka H, Okada M, Oshimura N, Tofuku A. Chromatic instabilities in cesium-doped tungsten bronze nanoparticles. Journal of Applied Physics. 2013;114.

[31] Liu G, Kong F, Xu J, Li R. Novel synthesis of 0D, 1D and 2D nano-CsxWO3 and their tunable optical-thermal response performance. Journal of Materials Chemistry C. 2020.

[32] Liu J, Xu Q, Shi F, Liu S, Luo J, Bao L, et al. Dispersion of Cs0.33WO3 particles for preparing its coatings with higher near infrared shielding properties. Applied Surface Science. 2014;309:175-80.

[33] Liu J, Luo J, Shi F, Liu S, Fan C, Xu Q, et al. Synthesis and characterization of F-doped Cs0.33WO3−F particles with improved near infrared shielding ability. Journal of Solid State Chemistry. 2015;221:255-62.

[34] Liu J, Ran S, Fan C, Qiao Y, Shi F, Yang J, et al. One pot synthesis of Pt-doped CsxWO3 with improved near infrared shielding for energy-saving film applications. Solar Energy. 2019;178:17-24.

[35] Ran S, Liu J, Shi F, Fan C, Yang J, Chen B, et al. Microstructure regulation of CsxWO3 nanoparticles by organic acid for improved transparent thermal insulation performance. Materials Research Bulletin. 2019;109:273-80.

[36] Cai L, Wu X, Gao Q, Fan Y. Effect of morphology on the near infrared shielding property and thermal performance of K0.3WO3 blue pigments for smart window applications. Dyes and Pigments. 2018;156:33-8.

[37] Zhao Z, Bai Y, Ning W, Fan J, Gu Z, Chang H, et al. Effect of surfactants on the performance

of 3D morphology W18O49 by solvothermal synthesis. Applied Surface Science. 2019;471:537-44.

Table 1

The optical parameters of the CWO-3/PVA composite films with different solid content

Solid content (wt%)	T_{Vis}[a] (%)	T_{NIR}[b] (%)	S_{NIR}[c] (%)	K[d]
2	81.31	24.11	75.89	3.37
4	72.65	16.06	83.94	4.52
6	71.76	14.36	85.64	4.99
8	68.80	13.55	86.45	5.08

[a] Average transmittance of visible light region (380-780nm): $T_{vis} = \frac{\int_{380}^{780} T(\lambda) d(\lambda)}{(780-380)\times 100} \times 100\%$,

$T(\lambda)$ is the function curve of spectral transmittance with wavelength as independent variable

[b] Average transmittance of near-infrared light region (780-2500nm): $T_{NIR} = \frac{\int_{780}^{2500} T(\lambda) d(\lambda)}{(2500-780)\times 100} \times 100\%$

[c] Average shielding ratio of near-infrared light region (780-2500nm): $S_{NIR} = 100\% - T_{NIR}$

[d] Spectrally selective index: $K = \frac{T_{vis}}{T_{NIR}}$

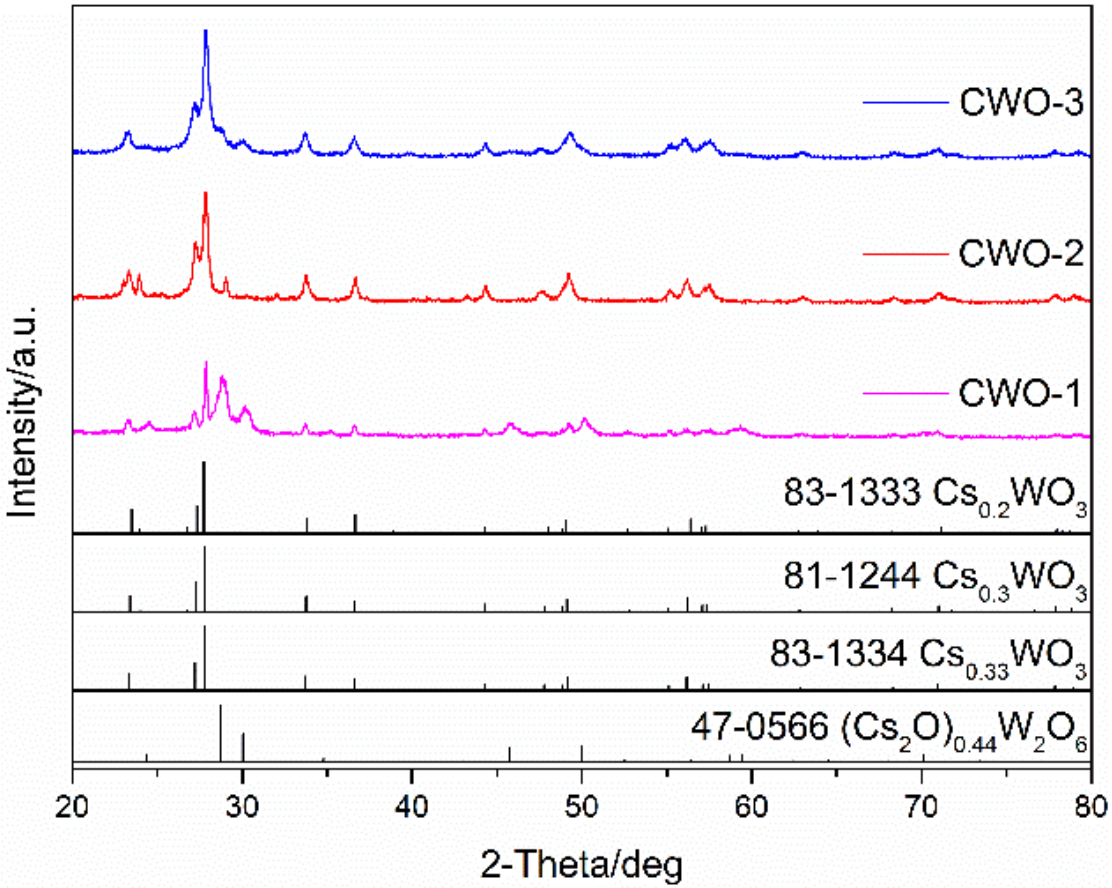

Fig. 1 XRD patterns of as-synthesized CWO-1, CWO-2 and CWO-3.

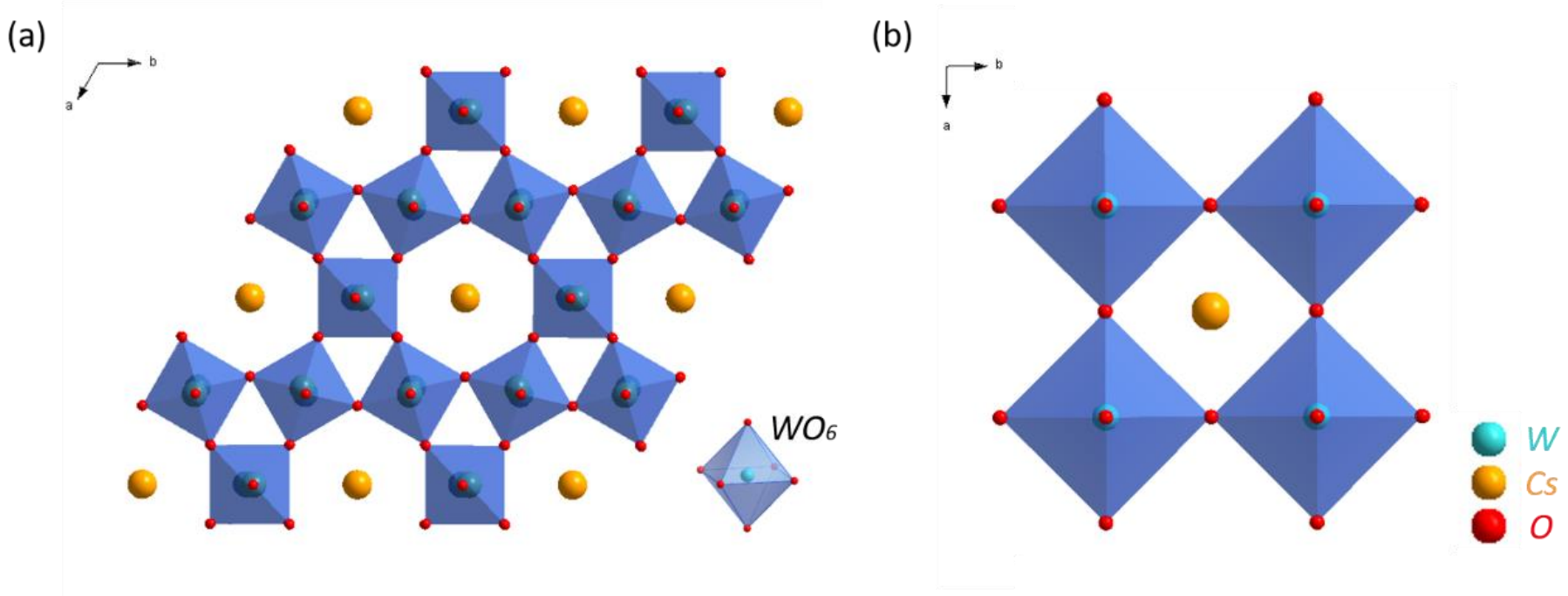

Fig. 2 Structural framework of (a) Cs-HTBs and (b) Cs-CTBs projected on *a*-*b* planes.

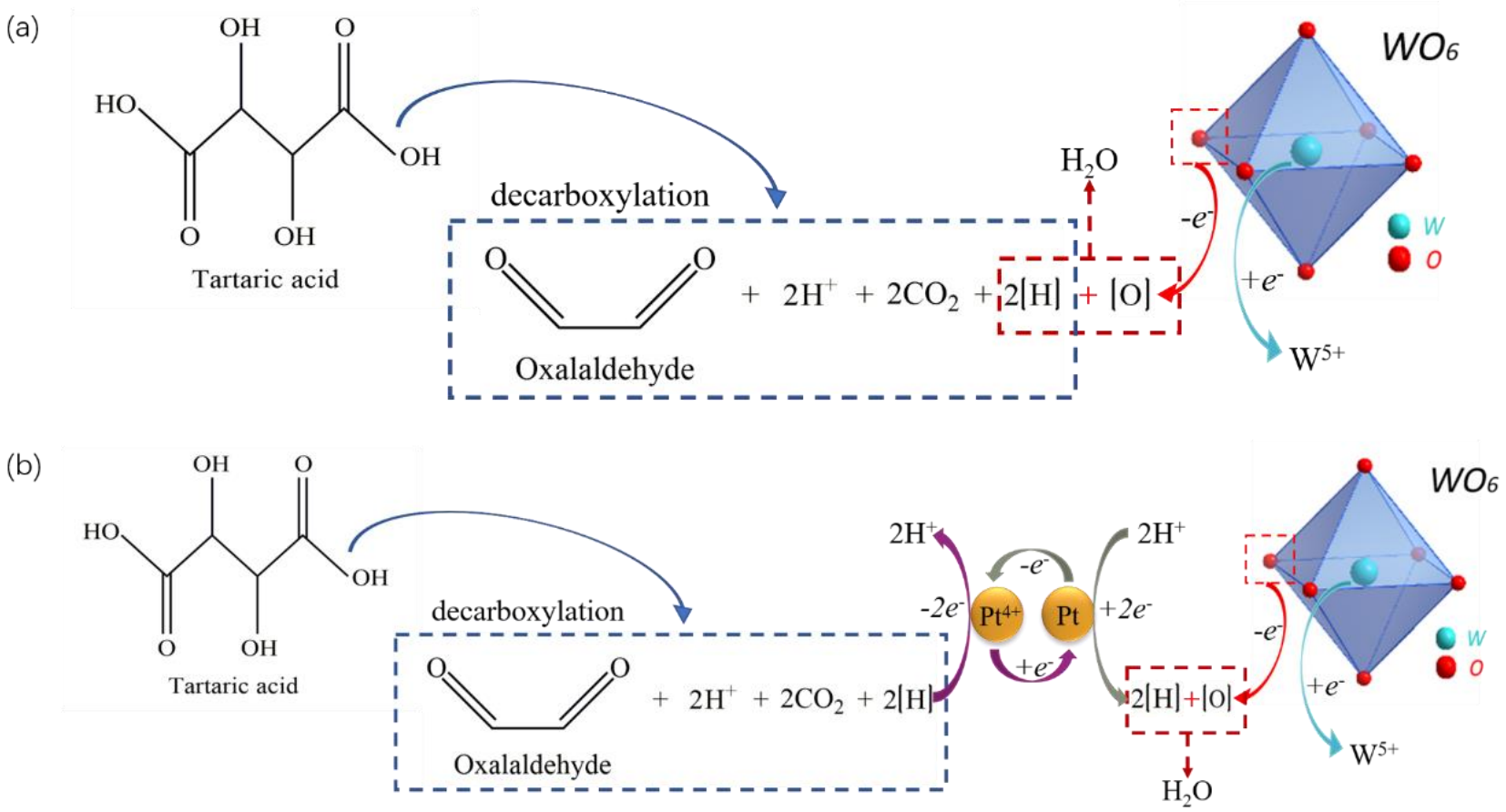

Fig. 3 The reaction diagram of reducing process under different reducing agents: (a) tartaric acid and (b) tartaric acid with chloroplatinic acid.

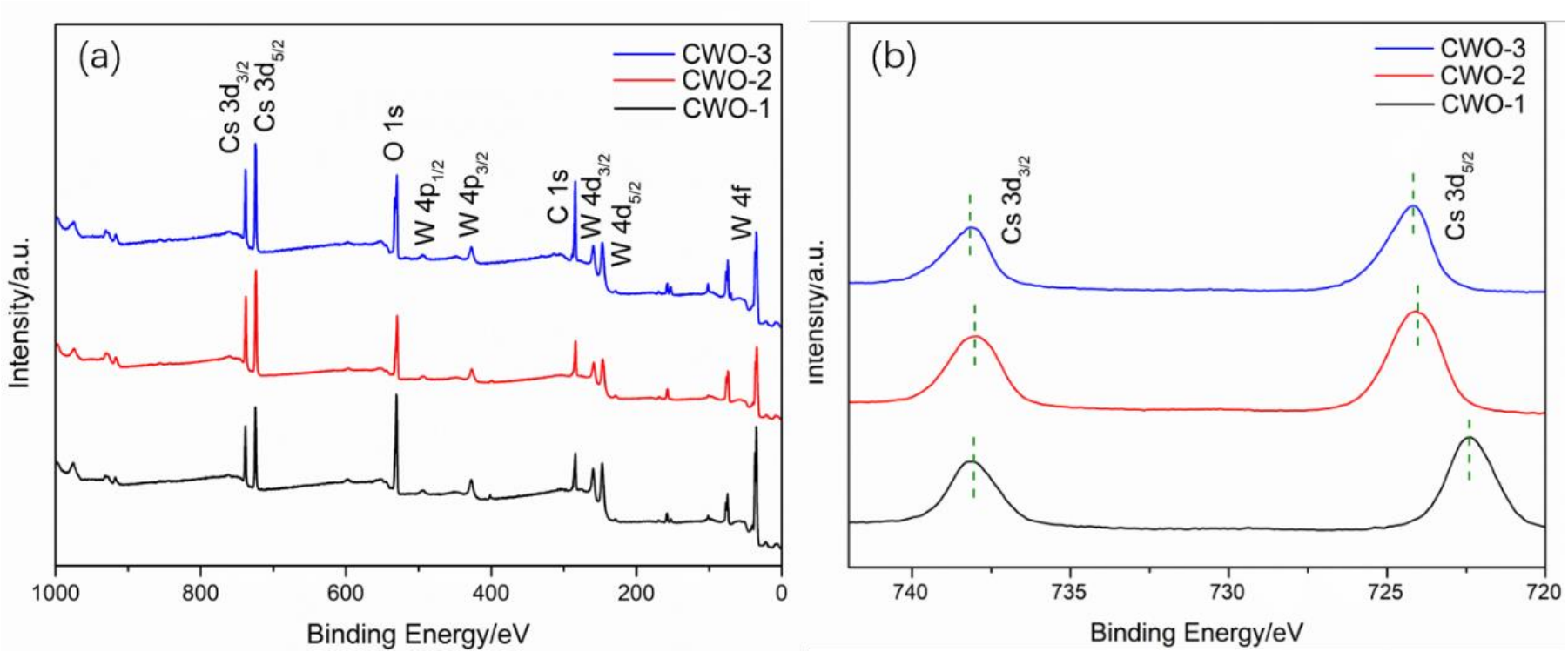

Fig. 4 (a) XPS survey spectra and (b) Cs 3d core-level spectra of CWO-1, CWO-2 and CWO-3

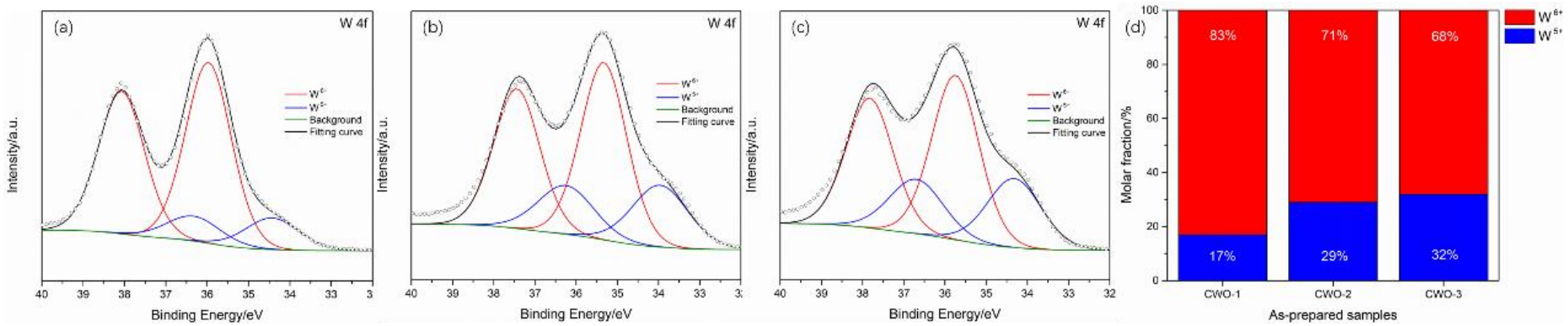

Fig. 5 The W4f core-level spectra of (a) CWO-1, (b) CWO-2 and (c) CWO-3; (d) The valence distribution of W element in CWO-1, CWO-2 and CWO-3.

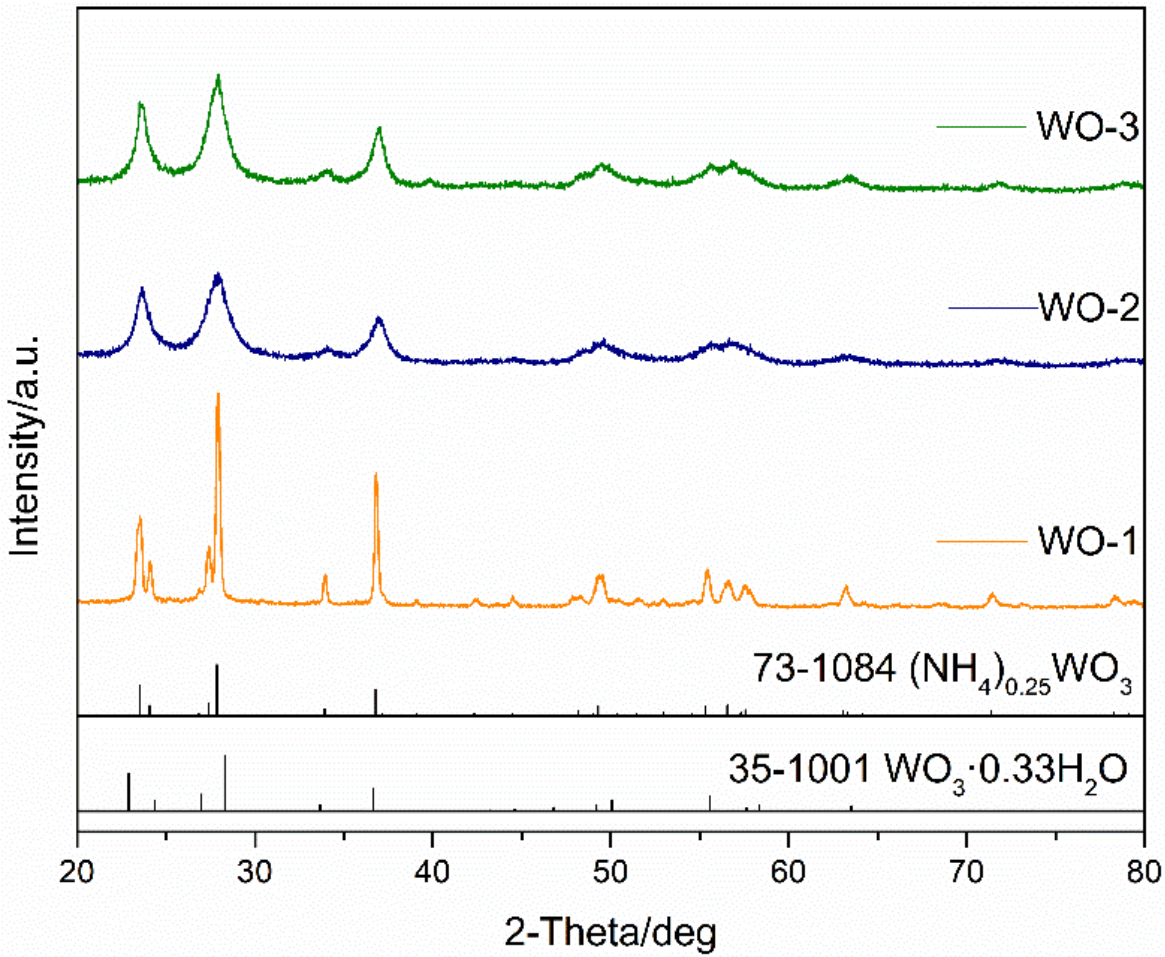

Fig. 6 XRD patterns of WO-1, WO-2 and WO-3.

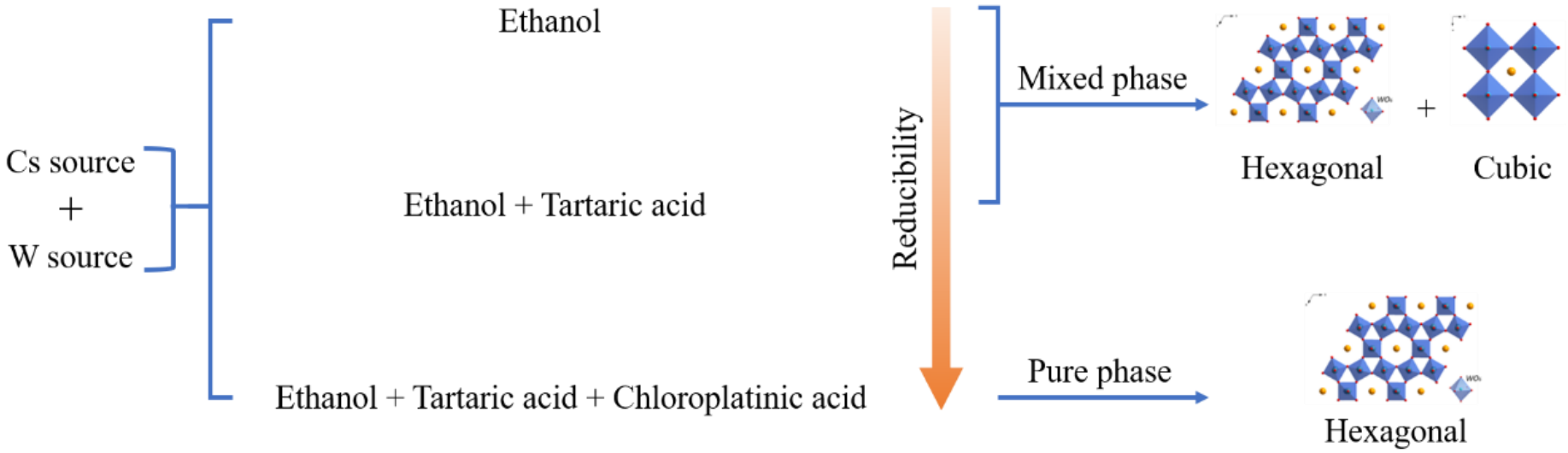

Fig. 7 Schematic diagram of the growth mechanism of as-synthesized nanocrystals with different phase composition.

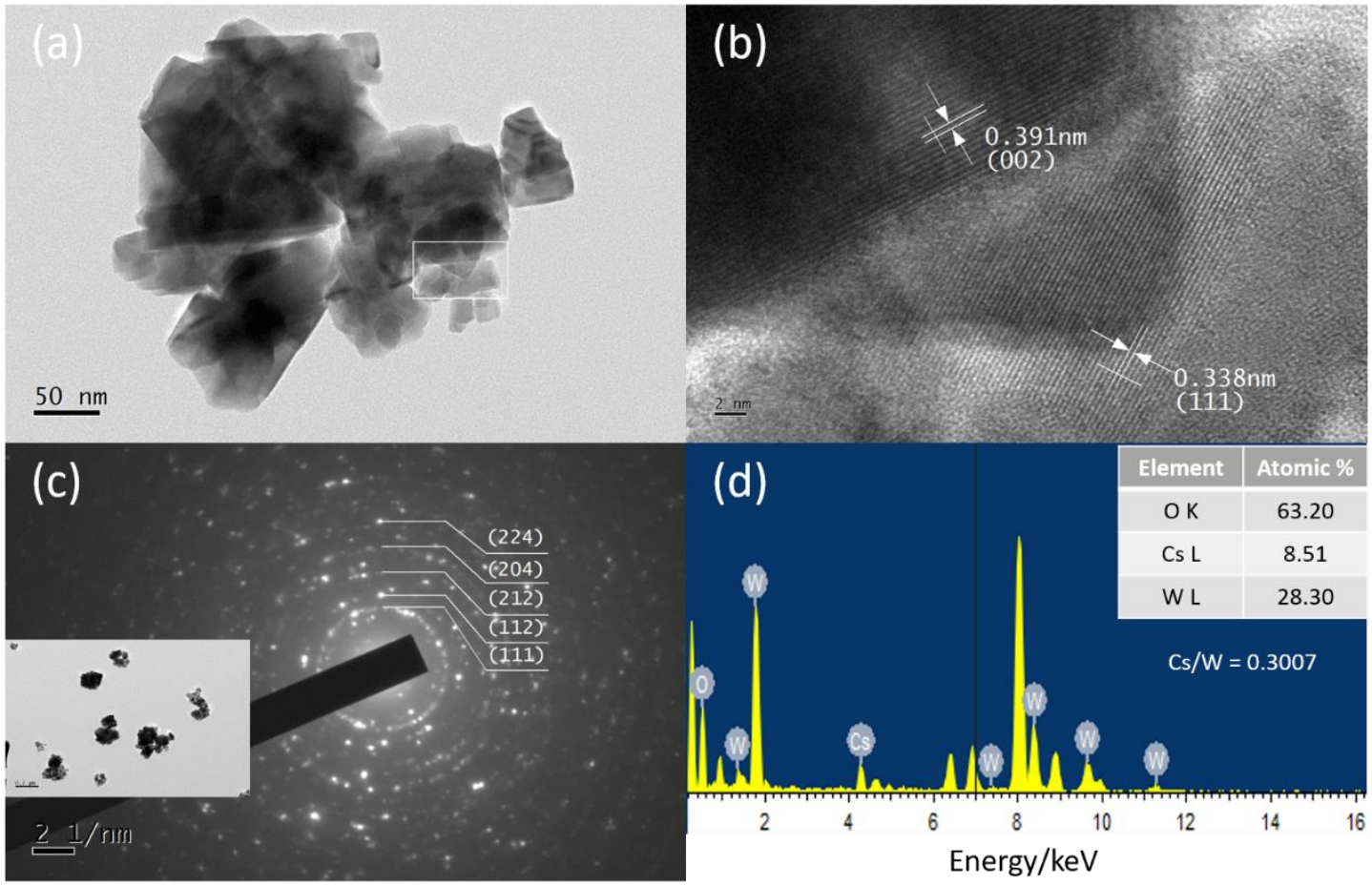

Fig. 8 (a) TEM image, (b) HRTEM image of selected area, (c) SAED pattern with diffraction area inset and (d) EDS pattern of CWO-3.

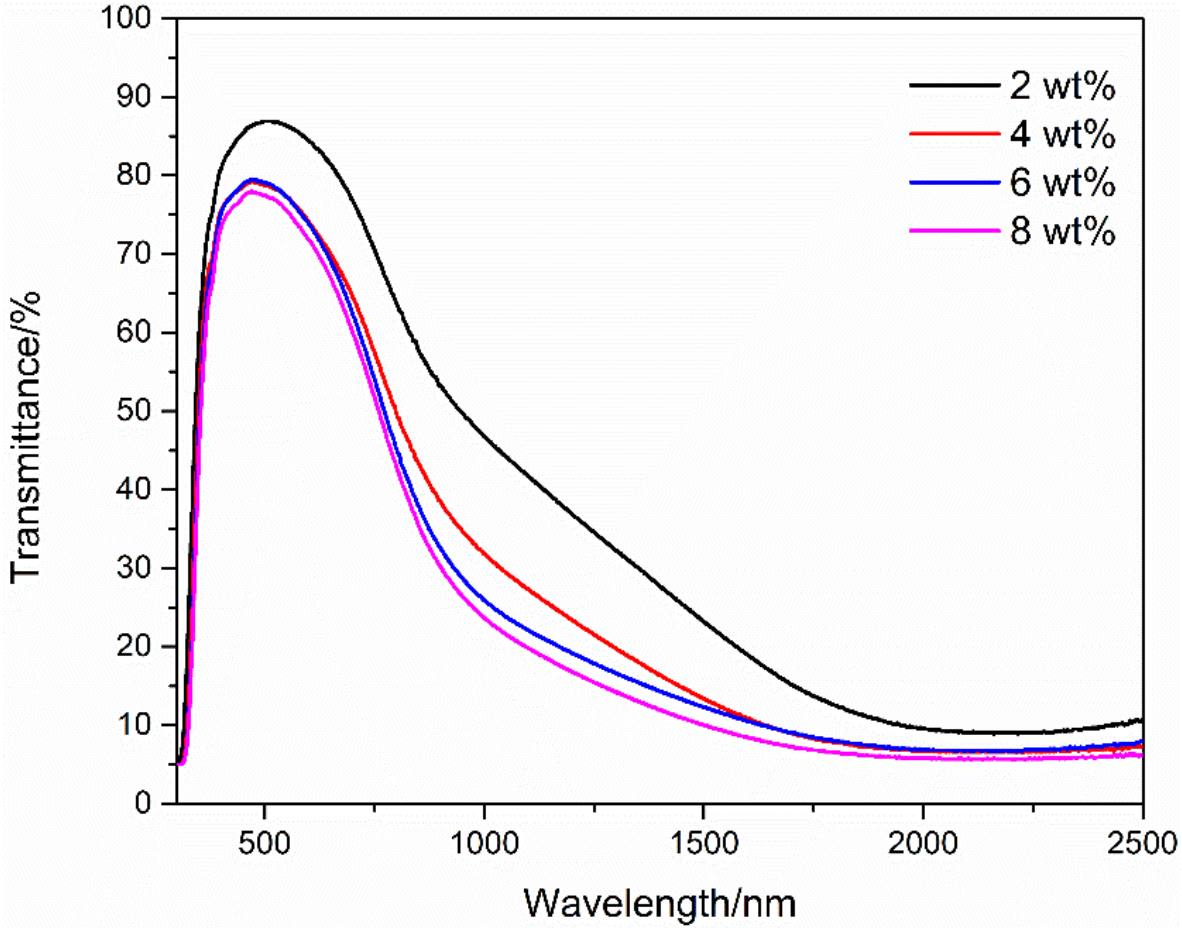

Fig. 9 UV-Vis-NIR transmittance spectra of the CWO-3/PVA composite films prepared by dispersions with different solid content.

Graphical Abstract